Applied Physics B (2018) 124:32
https://doi.org/10.1007/s00340-018-6901-5

Applied Physics B
Lasers and Optics

The phase interrogation method for optical fiber sensor by analyzing the fork interference pattern

Riqing Lv[1] · Liqiang Qiu[1] · Haifeng Hu[1] · Lu Meng[1] · Yong Zhang[1]

Received: 9 October 2017 / Accepted: 24 January 2018 / Published online: 1 February 2018

Abstract

The phase interrogation method for optical fiber sensor is proposed based on the fork interference pattern between the orbital angular momentum beam and plane wave. The variation of interference pattern with phase difference between the two light beams is investigated to realize the phase interrogation. By employing principal component analysis method, the features of the interference pattern can be extracted. Moreover, the experimental system is designed to verify the theoretical analysis, as well as feasibility of phase interrogation. In this work, the Mach–Zehnder interferometer was employed to convert the strain applied on sensing fiber to the phase difference between the reference and measuring paths. This interrogation method is also applicable for the measurements of other physical parameters, which can produce the phase delay in optical fiber. The performance of the system can be further improved by employing highlysensitive materials and fiber structures.

1 Introduction

Optical fiber sensors, with the advantages of small size, electromagnetic immunity and good corrosion resistance, had become excellent choices for measurements in harsh environments [1, 2]. With the rapid development of optical fiber sensors, many kinds of sensing structures based on optical fiber had been proposed, such as optical fiber Fabry–Perot (F–P) cavity, fiber Bragg grating (FBG), photonic crystal fiber (PCF) sensors and so on [3–6]. To improve the measurements, except developing better sensing structure, one should also consider applying novel interrogation method of the optical fiber sensing system. The sensing signals from these optical fiber structures mentioned above were always analyzed by intensity and wavelength interrogation methods. Generally speaking, the wavelength interrogation method was more preferred in optical fiber sensing technology, because the influence of the light power fluctuation in the sensing system could be significantly reduced. In this case, the resolution of the measurement depended on the wavelength resolution of the spectrometer. For precision measurements based on optical fiber sensors, a high-performance spectrometer is indispensable, which increased the cost of the sensing system largely. Other kinds of interrogation methods were still necessary to be explored, in order to give another option to analyze the sensing signal from optical fiber.

In this work, based on fork interference pattern of orbital angular momentum (OAM) beam and plane wave, the phase interrogation method for fiber Mach–Zehnder interferometers (MZI) is proposed. The feature of the fork interference pattern is extracted by principal component analysis (PCA) method, and the relationship between the phase difference and the variation of the fork pattern is investigated. In this method, the power of incident light does not affect the main feature of the interference pattern, so the influence of the light power fluctuation can be eliminated. Moreover, compared with the wavelength interrogation systems by employing spectrometers, the requirement of the incident light power is rather low in the proposed method, and the system is simple and low cost. The theoretical resolution of this method is estimated to be 0.0636 με, which depends on the parameters of the imaging system and the fiber properties. The experimental system is built to verify our design. In the reference path of the fiber interferometer, the OAM beam is emitted from the two-mode fiber (TMF) after mode conversion processes [7]. The plane wave is generated by collimating the emitted light from single mode fiber (SMF) in the measuring path. The interference pattern of the two beams is recorded by the charge-coupled device (CCD) camera. In order to characterize the sensing performance of the system,

---

✉ Haifeng Hu
huhaifeng@ise.neu.edu.cn

[1] College of Information Science and Engineering, Northeastern University, Shenyang 110819, China

strain is applied on sensing fiber in the measuring path to change the phase delay in the MZI. The features of the fork interference patterns under different strain are extracted. It should be noticed that, except strain, other parameters with the ability to modify the light phase delay in fiber can also be measured by this interrogation method.

2 Theoretical analysis

2.1 System design

To realize the phase interrogation, the fiber MZI is designed as shown in Fig. 1. By the 3 dB optical coupler (OC), the light emitted from laser source is divided into two parts which are transmitted in the measuring path and reference path, respectively. In the reference path, the OAM beam is generated in two modes fiber by the mode converter, whose working principle will be discussed in Sect. 3.1. In the measuring path, the plane wave can be approximately obtained by collimating the light emitted from the end of SMF. By using a beam-splitting cube, the interference pattern of the light beams from the two paths can be formed and recorded by the CCD camera. The angle between the two beams can be adjusted by rotating the reflector. When the incident light passes through the sensing fiber in the measuring path, the phase delay can be modified by the variation of the stress on fiber. The relationship between the interference pattern and the phase delay is investigated. After that, the phase interrogation method by analyzing the digital interference pattern is verified, when applied in sensing system. The principles of interference pattern and the phase interrogation will be explained in the next two sections.

2.2 Fork interference pattern

OAM beam is characterized by a helical phase front of $\exp(il\varphi)$, in which φ refers to the azimuth angle and l is the topological charge [8, 9]. Because of the helical phase structure, it has the doughnut shape intensity profile with a phase singularity point at the beam center. Driven by the unique properties, OAM beam has been widely used in particle manipulation, optical tweezers and optical communications [10–12]. In this work, the distinctive interference pattern of OAM beam and plane beam is employed to demodulate the sensing signal. According to the interference theory [13], the intensity distribution between two light beams can be expressed by Eq. (1)

$$I(r,\varphi) = \left|E_1(x,y) + E_2(x,y)\right|^2, \tag{1}$$

where $E_1(x, y)$ and $E_2(x, y)$ are the electric field distributions of the OAM beam and plane wave. For the OAM beam with $l=1$, the electric field on x–y plane can be expressed by Eq. (2):

$$E_1(r,\varphi) = A_1(r)\exp(il\varphi), \tag{2}$$

where A_1 is the amplitude distribution. Due to the helical phase structure, it is convenient to describe the electric field of OAM beam in polar coordinate (r, φ). In this case, the center of the beam is located at $r=0$. The intensity and phase distribution of the OAM beam with $l=1$ is shown in Fig. 2a, b.

For plane wave with the propagation direction of $(\sin\beta, 0, \cos\beta)$, the electric field on x–y plane can be expressed as

$$E_2(x,y) = A_2(x,y)\exp(ikx\sin\beta + i\phi), \tag{3}$$

where $A_2(x, y)$ is the amplitude distribution of the plane wave, and k refers to the plane wave numbers, β refers to the angle between the direction of plane wave propagation and z-axis. ϕ is the additional phase delay, which is equivalent to the phase difference between OAM beam and plane wave in the theoretical analysis of next section. The intensity and phase distribution of the plane wave is shown in Fig. 2c, d. In this work, the plane wave is generated by collimating the light from optical fiber, so the intensity distribution is Gauss

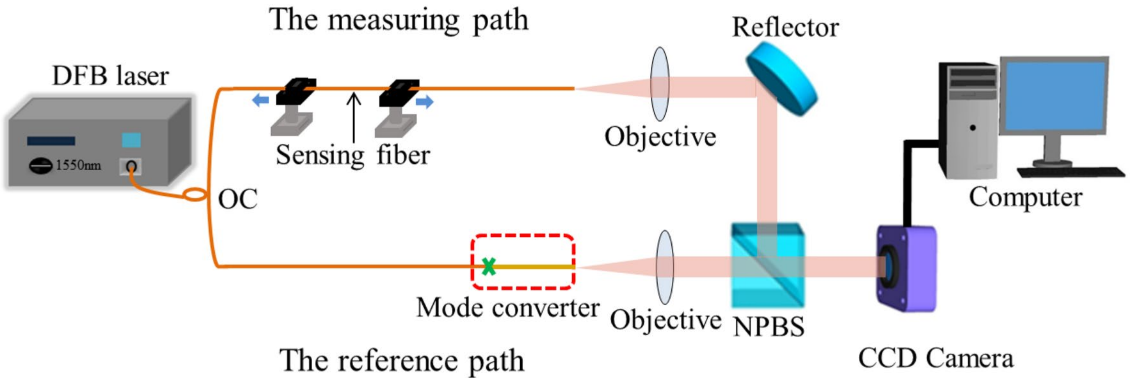

Fig. 1 The schematic diagram of the phase interrogation method based on the OAM beam

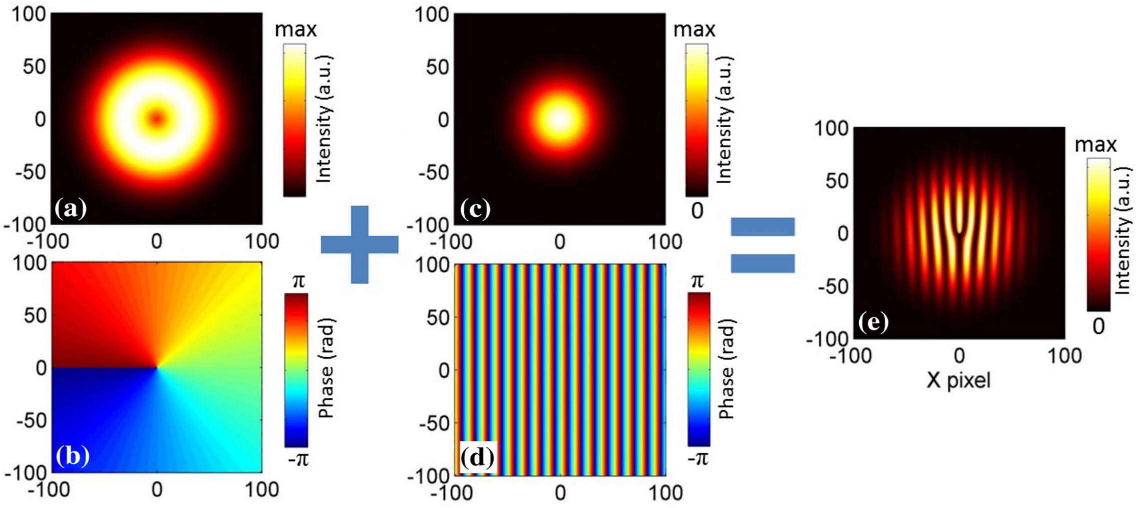

Fig. 2 The intensity and phase distribution of OAM beam with $l = 1$ in **a, b**. The intensity and phase distribution of plane wave in **c, d**. The interference pattern by the OAM beam and plane wave with the phase difference of ϕ in **e**

type. When the two beams interfere with each other, the interference pattern of the light intensity is shown in Fig. 2e, which exhibits a fork shape at the OAM beam center.

2.3 Principle of phase interrogation

When the phase difference between the two beams is modified, the shape of fork pattern is changed. The interference pattern under the phase difference from $\phi = 0°$ to 315° is shown in Fig. 3a–h, respectively. The interval of phase difference between each two adjacent pattern is 45°.

The obvious change near the branch point of the fork pattern can be recognized in Fig. 3. In this part, the relationship between the interference pattern and phase difference is investigated. To speed the image processing, the method to quantitatively evaluate the feature of the pattern is proposed based on PCA in this work [17]. PCA is linear transformation method based on the statistical techniques, which can be applied in digital image processing (e.g., face recognition). In this work, it is employed to realize the pattern recognition. By reducing the data dimension, the speed of the digital image process can be largely increased. The obtained principal components can reflect the features of the original image. Each

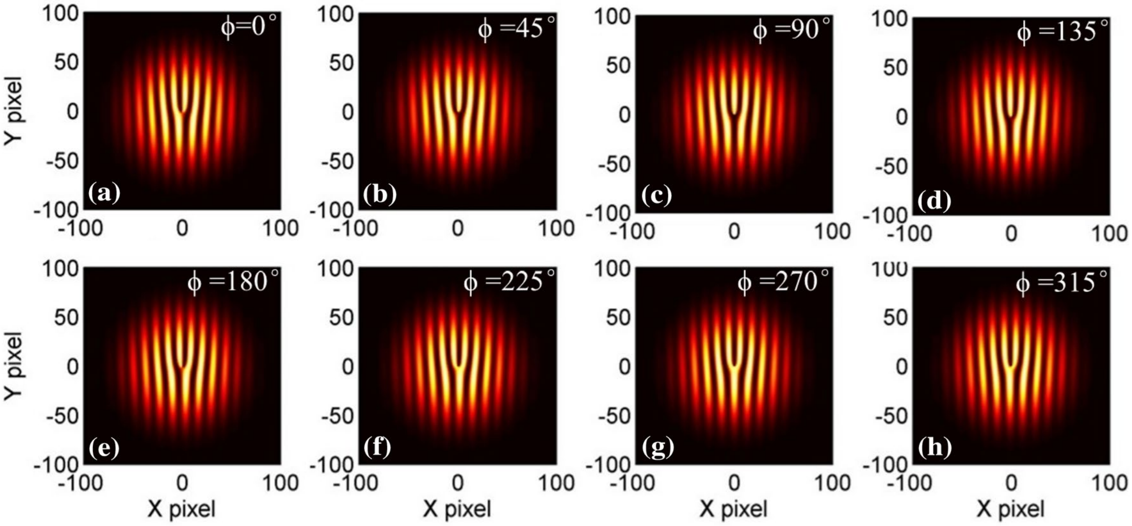

Fig. 3 The interference patterns by the OAM beam and plane wave under different phase differences. **a** $\phi = 0°$, **b** $\phi = 45°$, **c** $\phi = 90°$, **d** $\phi = 135°$, **e** $\phi = 180°$, **f** $\phi = 225°$, **g** $\phi = 270°$, **h** $\phi = 315°$

image is a two-dimensional array of 200×200 intensity values (8-bit), which can be transformed into a column vector with $N^2\times 1$ dimension. In order to perform the recognition, 37 patterns with different ϕ from 0° to 720° calculated by Eq. (1) are chosen as the initial set of the patterns (i.e., the training set). The interval of the phase difference ϕ is 20°. The pattern set is represented by $\mathbf{\Phi} = [\mathbf{\Phi}_1, \mathbf{\Phi}_2, \mathbf{\Phi}_3, \ldots\mathbf{\Phi}_M]$, where $M=37$ is the total number of patterns. Each $\mathbf{\Phi}_i$ has been subtracted by the average vector of these patterns. Then, the eigenvalues and eigenvectors of covariance matrix are calculated. The covariance matrix is defined by $C=\mathbf{\Phi}^{\mathbf{T}}\mathbf{\Phi}$, which is one $M\times M$ matrix. Among these eigenvalues, one can find that only two values are dominant, which are $\lambda_1=1.57\times10^4$ and $\lambda_2=1.49\times10^4$, and other eigenvalues are near-zero values. The eigenvalues indicate their contributions to characterize the features of the training patterns are great. In this case, the two eigenvectors, $\mathbf{V}_1$ and $\mathbf{V}_2$, corresponding to the principal eigenvalues are considered in the following process. Therefore, using PCA method, the dimensionality of the training pattern set can be largely reduced. Similar with the concept of eigenfaces in face recognition process [14], we define the eigenpatterns of the training set in Eq. (4):

$$[\,\mathbf{U}_1\;\;\mathbf{U}_2\,] = \mathbf{\Phi}\times[\,\mathbf{V}_1\;\;\mathbf{V}_2\,]. \tag{4}$$

Figure 4a, b shows the two eigenpatterns, which are obtained by reshaping $\mathbf{U}_1$ and $\mathbf{U}_2$ to be matrixes with the size of 200×200, respectively. The two eigenpattern vectors can be considered as the base vectors to define a new two-dimensional space. One pattern ($\mathbf{\Phi}_i$) with arbitrary phase difference ϕ_i can be projected into this defined space by the following operation in Eq. (5):

$$\Omega_i = \begin{bmatrix}\omega_1\\ \omega_2\end{bmatrix} = \begin{bmatrix}\mathbf{U}_1^T\\ \mathbf{U}_2^T\end{bmatrix}\mathbf{\Phi}_i. \tag{5}$$

From Fig. 4, one can recognize that, near the branch point of the fork patterns $\mathbf{U}_1$ has the anti-symmetric distribution, and $\mathbf{U}_2$ has the symmetric distribution. So the vector of $\mathbf{\Omega}$ can be used to evaluate the degree of symmetry of an interference pattern.

When ϕ_i equals to a series of value from 0° to 340°, the corresponding points of Ω_i are plotted in the ω_1–ω_2 plane as shown in Fig. 5a. From the calculation results, the position of Ω_i point rotates around the original point of ω_1–ω_2 plane in the clockwise direction. Therefore, the argument of Ω_i is employed to represent the main feature of the interference pattern between the OAM beam and plane wave. The relationship between the light phase difference and the argument of

Fig. 4 The two principal eigenpatterns for the training set of 37 patterns with different ϕ values

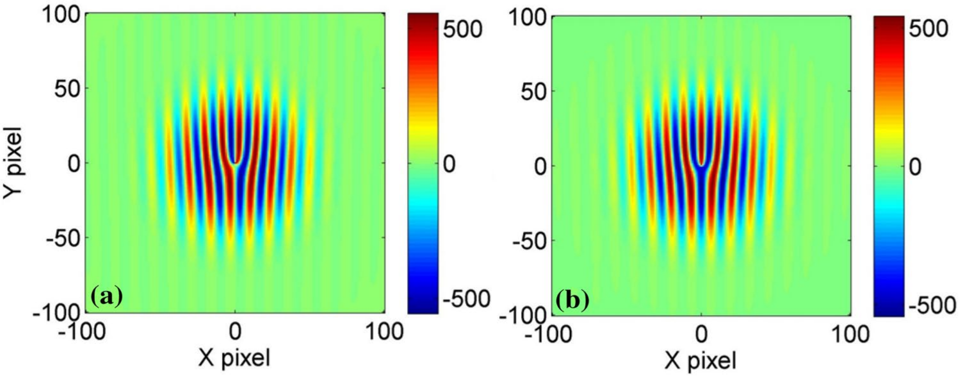

Fig. 5 **a** The position of Ω_i in the ω_1–ω_2 plane, when $\phi=0°$, 20°, 40°, …, 340°. **b** The relationship between the phase difference ϕ and the argument of Ω_i

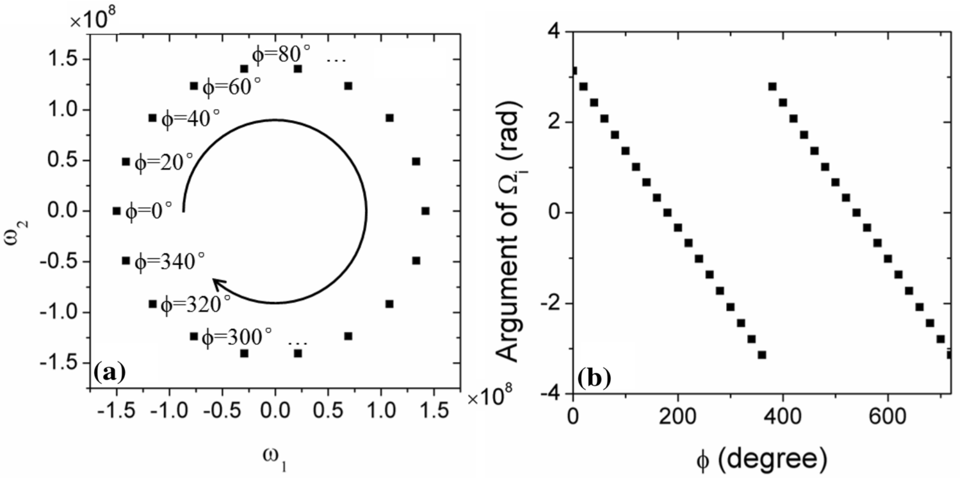

Ω_i is shown in Fig. 5b. In Fig. 5b, all the 37 patterns in the training set are processed by Eq. (5). The phase difference ϕ ranges from 0° to 720°. Due to the wrapped phase effect, the argument value is restricted in $[-\pi, \pi]$, which also limits the dynamic measuring range of this phase interrogation method. Within the range of [0°, 360°], there was a good linear relationship between phase difference ϕ_i and the argument of Ω_i. Specifically, the relationship is $\Omega_i = 180° - \phi_i$. This interrogation method can be applied in the optical fiber sensing technology. When the variation of the experimental parameter can influence the propagation phase delay in optical fiber, this phase delay can be monitored by analyzing the interference pattern. The image analysis process only requires the operation of Eq. (5), when the two eigenpattern vectors are already determined by the training set. The efficient method is helpful to measure the phase difference between the measuring path and the reference path in real time.

2.4 The principle of strain measurements

In this work, the strain measurement is carried out to verify the phase interrogation method. When the stress is applied on optical fiber, the phase delay of the propagating light can be generated. By considering the length variation and the elasto-optic coefficient of fiber, the phase delay can be expressed by Eq. (6):

$$\Delta\phi = n\frac{2\pi}{\lambda}L\left\{1 - 0.5n^2\left[(1-\nu)p_{12} - \nu p_{11}\right]\right\}\varepsilon \qquad (6)$$

Here λ is the wavelength of the light source, L is the length of the fiber under strain, n is the effective refractive index of the fiber mode, p_{11} and p_{12} are the elasto-optic coefficient of the fiber, ν is the Poisson's ratio, and ε is the strain. Therefore, there is a linear relationship between phase delay and applied strain on optical fiber. In the following experiments, the strain on optical fiber is converted to light phase difference by fiber MZI. Finally, the phase difference can be determined by image processing method based on PCA.

3 Experimental results

3.1 The OAM mode conversion

The OAM mode converter is an important part of the proposed system. There have been many attempts to generate and manipulate OAM beam. In free space, there are some optical devices to realize the OAM beam conversion, such as phase plates, cylindrical lenses, and spatial light modulators. Meanwhile, there is increasing interest in the generation of OAM beams in optical fibers [15, 16], because the OAM modes are intrinsic high order modes in optical fiber. To be compatible with the fiber-sensing structure, a kind of OAM mode converter based on the all fiber structure is proposed in this work as shown in Fig. 6a. Under the weak-guidance approximation condition, linearly polarized (LP) modes can be obtained by solving the scalar wave equation for optical fiber. There are two indices to describe LP_{lm} mode, where l is the azimuthal index and m is the radial index. Each LP_{lm} with $l > 0$ consists of twofold degenerate modes labeled by a and b, respectively. The OAM modes can be obtained by combining the two degenerate LP_{lm} modes with $\pi/2$ or

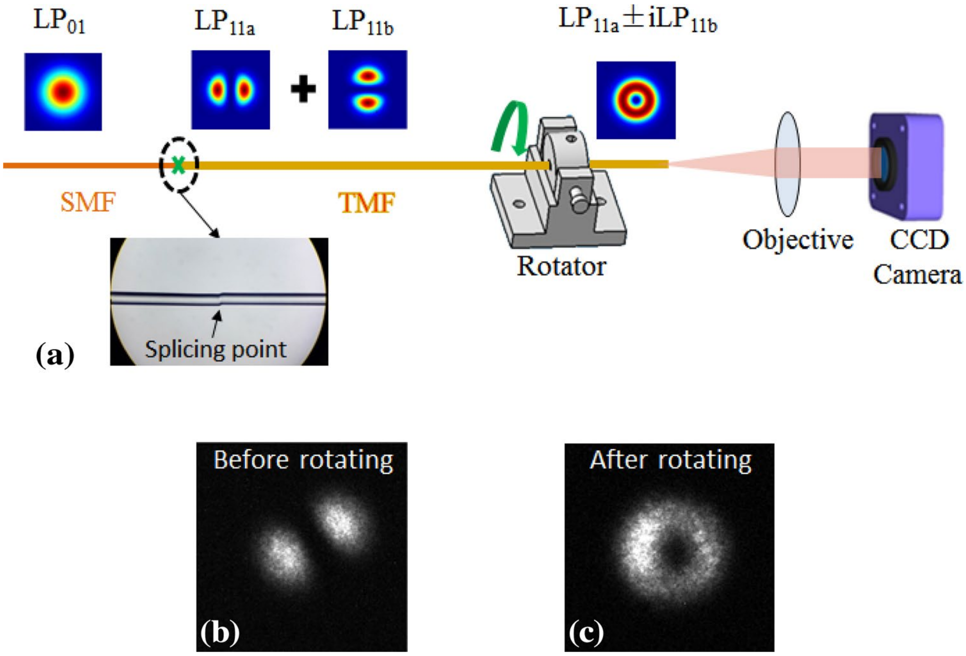

Fig. 6 **a** The schematic diagram of OAM mode converter. **b** The beam profile of LP_{11} mode measured by CCD camera before rotating. **c** The beam profile of OAM mode measured by CCD camera after rotating

$3\pi/2$ phase difference (i.e., OAM = $LP_{lma} \pm i \times LP_{lmb}$). For example, the OAM mode with $l = 1$ can be generated by the combination of LP_{11a} and LP_{11b} modes in TMF, which can support LP_{01} and LP_{11} modes [17]. Therefore, the LP_{01} mode, which cannot contribute to the OAM mode, should be suppressed in TMF. In the previous work, long-period grating is inscribed in TMF to convert the LP_{01} mode to LP_{11} mode at the resonance wavelength of the long-period grating [17]. This conversion process is efficient, but the operating wavelength is difficult to adjust. In this work, FMF is spliced to lead-in SMF with the core-offset of 15 μm. In this structure, when the LP_{01}-mode incidents from SMF, the power ratio between LP_{11} and LP_{01} is above 20 dB in C-band (λ is from 1520 to 1570 nm) according the theoretical simulation. Therefore, the LP_{11} mode can be excited in FMF for a broadband wavelength range by the highly asymmetric structure in Fig. 6b. However, the phase difference between LP_{11a} and LP_{11b} modes is unknown. In order to obtain OAM mode, the rotator is employed in the system to clamp the TMF and apply a twist on the fiber, which can modify the phase difference between LP_{11a} and LP_{11b} modes. During rotating the fiber, the near-field field profile is monitored by CCD camera. In the experiment, the length of the twisted TMF is 25 cm. When the rotating angle is 45° approximately, the light beam with the annular intensity profile is obtained in Fig. 6c.

3.2 The experimental setup

To verify the feasibility of the phase interrogation method, the sensing section in the measuring path is applied by stress. Both the measuring path and reference path are placed in the same environment simultaneously to eliminate the influence of temperature variation. As mentioned above, the strain causes the phase delay between the two paths of the Mach–Zehnder interferometer. In this case, the strain signal is converted to shape variation of the interference pattern, which is real-time monitored by the CCD camera. The information of the recorded digital image is extracted by the image processing method based on PCA as discussed in Sect. 2.3.

The photograph of the optical fiber strain sensing experiment system is shown in Fig. 7. In the system, distributed feedback (DFB) laser with linewidth of 3 MHz with a central wavelength of 1550 nm is used as the light source. The optical coupler is a 2 × 2 single-mode fiber coupler with splitting ratio of 1:1. The core diameters of SMF and TMF are 8.2 and 15 μm. The refractive index differences between the core and cladding of the two kinds of fiber are both $(n_1 - n_2)/n_1 = 0.336\%$. FMF is spliced to SMF with the core-offset of 15 μm. The splicing point is protected by epoxy resin and fixed by a holder. The length between the holder and the rotator is 25 cm. the output beams of SMF and TMF are collimated by 20 × objective lens. The non-polarized beam splitter (NPBS) is employed to generate the inference pattern on the CCD camera, whose maximum resolution is 1296 × 964. The fork interference pattern is obtained when the incident light power is 10 μW, which indicates that the sensing system is low power consumption.

During the measurement, a segment of SMF on the measuring path is clamped by two fiber holders, which are fixed on two movable stages, respectively. The stress is applied on the fiber by stretching the fiber along the axial direction. At the same time, the shape variation of the fork interference pattern

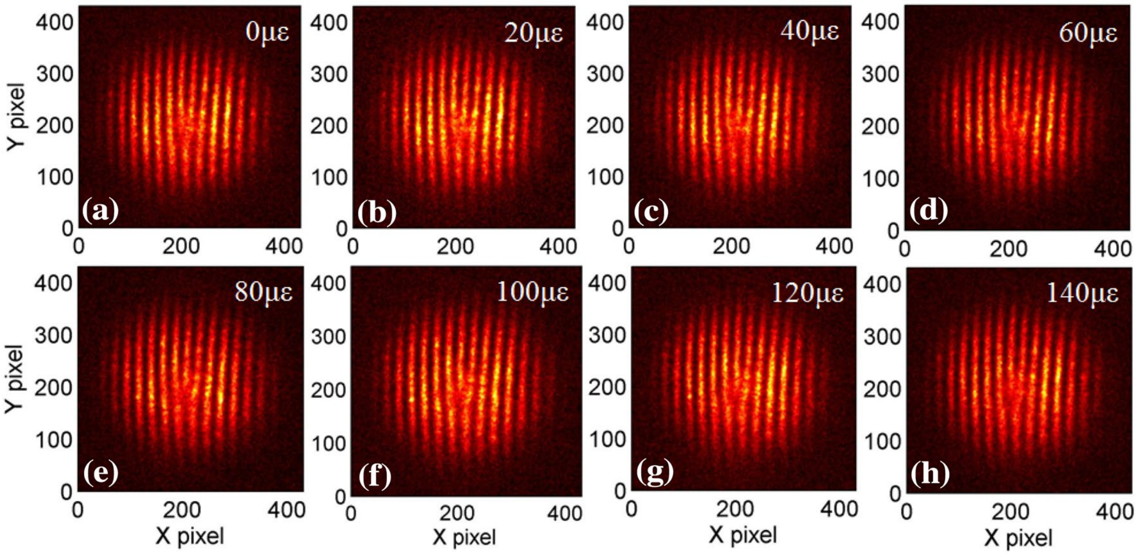

Fig. 7 Interference pattern for different strains applied on the sensing fiber. **a** 0 με, **b** 20 με, **c** 40 με, **d** 60 με, **e** 80 με, **f** 100 με, **g** 120 με, **h** 140 με

is recorded on the CCD. Before the feature extraction, preprocessing is required to enhance the image quality. The median filter and mean filter are both used to process the fork interference patterns obtained in the experiment. The filter template size is 3 × 3. In the experiments, the length between the two fiber holders is 50 cm, and the minimum moving distance of the stages is 10 μm. In this experimental system, the minimum strain of 20 με can be provided. When the applied strain on optical fiber is changed from 0 to 240 με, the corresponding 13 interference patterns are recorded. The first 8 patterns are shown in Fig. 8. From the shape of the patterns, the branch point can be recognized in each pattern. It can be proved that the OAM beam with $l = 1$ is generated in the mode conversion process. The similar shape evolution process as the simulated results in Fig. 3 can be recognized, which indicates that the applied stress can modify the phase difference between two paths. It should be mentioned that, due to the small area of the interference patterns, the region of interest with the size of 430 × 430 is picked up to accomplish the following analysis.

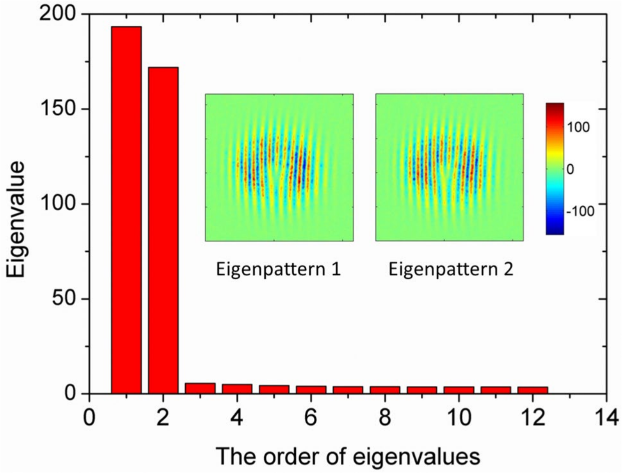

Fig. 8 The contribution rates of the eigenpatterns of the experimental images. Insets are the two eigenpatterns of λ_1 and λ_2

3.3 Sensing performance

The PCA in Sect. 2.3 is used to analyze the fork interference pattern measured above. The eigenvalues representing the contributions of all the eigenpattern are shown in Fig. 8. The sum of contribution rates by the first two eigenpattern (i.e., principal components) is 89.9%, which is lower than the theoretical results (nearly 100%). This may be caused by the image distortion and the serious noise of the near infrared CCD camera. The two eigenpatterns of λ_1 and λ_2 (as shown in the insets of Fig. 8) are obtained for further analysis of the fork interference patterns. Then each image is projected into the (ω_1, ω_2) space by the linear transformation of Eq. (5). The results of PCA when the fiber is under different strain are shown in Fig. 9a, b. In ω_1–ω_2 plane, Ω_i point experience the circular motion around the original point as predicted in Fig. 5a, when the strain on fiber is increased. Therefore, the argument of Ω_i is still selected to characterize the shape of each pattern. When the strain continues to increase, the argument of Ω_i may be outside that range from $-\pi$ to π. However, the calculated value by the arctangent function will be still wrapped within the range of $[-\pi, \pi]$. When the sampling rate is sufficiently high and the noise level is low, the algorithm of one-dimensional phase unwrapping can be employed to increase the dynamic sensing range [18].

To evaluate the sensitivity of this interrogation method, the linear fitting is used as shown in Fig. 10. The fitting curve can be expressed as Eq. (7), which indicates that the sensitivity is 0.04688 rad/με:

$$Y = 0.04688X + 2.5457. \tag{7}$$

When the strain is further increased (i.e., larger than 240 με), the interference pattern recorded by CCD becomes

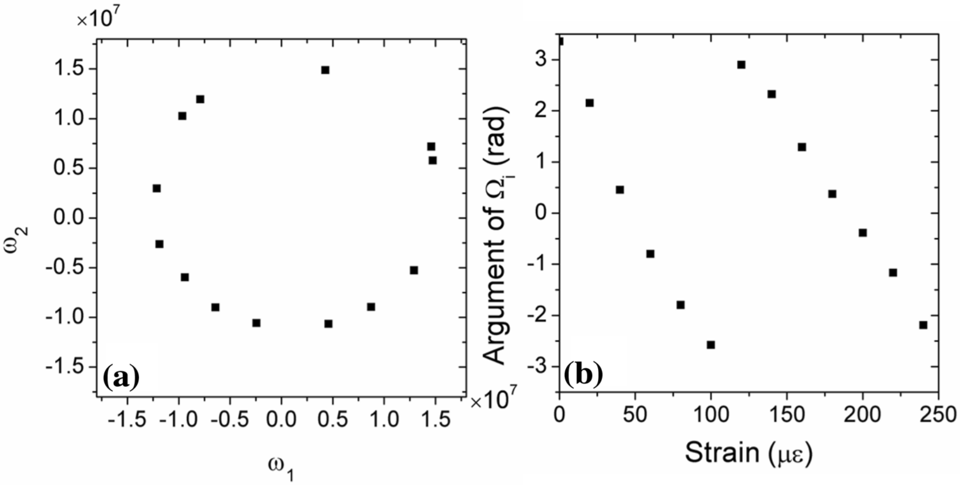

Fig. 9 **a** The position of Ω_i in the ω_1–ω_2 plane, when the applied strain ranges from 0 to 240 με. **b** The relationship between the applied strain on optical fiber and the argument of Ω_i

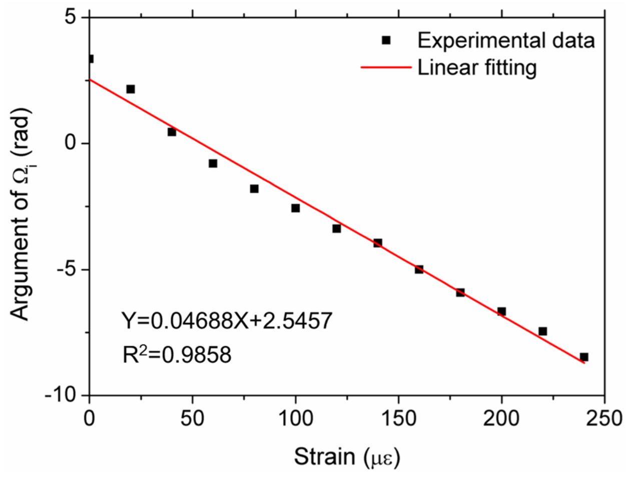

Fig. 10 The linear fitting results of the measured results processed by PCA

unstable over time. This may be explained by the viscoelastic nature of the polymer coating layer of optical fiber under large strain. The theoretical design of the phase interrogation method is verified by the strain-sensing experiments. The resolution of the experimental system is mainly affected by parameters of the imaging system and CCD camera. It should be noted that the bare optical fiber structure is employed as the sensing section without any process to increase sensitivities. If the more sensitive materials and fiber structure is introduced, the sensitivity and the resolution would be further improved.

4 Conclusion

In this work, the phase interrogation method based on OAM beam for optical fiber sensor is proposed and discussed. The feasibility of the proposed strain sensor has been verified by the simulation and experiments. PCA method is developed to extract the main features of the fork interference patterns. The patterns can be projected into a two-dimensional space by a simple linear transformation. The theoretical design is verified by the experiments of strain sensing. The sensitivity of the strain measurement is 0.04688 rad/με. It is possible to increase the sensitivity and the resolution of the proposed strain sensor by improving the sensitive material and the parameters of the structure. With the advantage of high-resolution, real-time measurement and low power consumption, the proposed method has a great application potential in industrial fields required high-resolution strain sensing.

Acknowledgements This work was partially supported by the National Nature Science Foundation of China (NSFC) (61403074) and the Fundamental Research Funds for the Central Universities (N160404002).

References

1. B. Li, L. Jiang, S. Wang, H.L. Tsai, H. Xiao, Femtosecond laser fabrication of long period fiber gratings and applications in refractive index sensing. Opt. Laser Technol. **43**(8), 1420–1423 (2011)
2. Y. Zhao, R. Lv, Y. Ying, Q. Wang, Hollow-core photonic crystal fiber Fabry-Perot sensor for magnetic field measurement based on magnetic fluid, Opt. Laser Technol. **44**(4), 899–902 (2012)
3. D.W. Duan, Y.J. Rao, Y.S. Hou et al., Microbubble based fiber-optic Fabry-Perot interferometer formed by fusion splicing single-mode fibers for strain measurement. Appl. Opt. **51**(8), 1033 (2012)
4. S.M. Lee, S.S. Saini, M.Y. Jeong, Simultaneous measurement of refractive index, temperature, and strain using etched-core fiber bragg grating, Sens. IEEE Photon. Technol. Lett. **22**(19), 1431–1433 (2010)
5. W. Li, C. Xu, S. Ho et al., Monitoring concrete deterioration due to reinforcement corrosion by integrating acoustic emission and FBG strain measurements. Sensors **17**, 657 (2017)
6. K.K. Qureshi, Z. Liu, H.Y. Tam et al., A strain sensor based on in-line fiber Mach–Zehnder interferometer in twin-core photonic crystal fiber. Opt. Commun. **309**(22), 68–70 (2013)
7. S. Li, Q. Mo, X. Hu et al., Controllable all-fiber orbital angular momentum mode converter. Opt. Lett. **40**(18), 4376–4379 (2015)
8. A.M. Yao, M.J. Padgett, Adv. Opt. Photon. **3**, 161 (2011)
9. L. Allen, M.W. Beijersbergen, R.J.C. Spreeuw, J.P. Woerdman, Phys. Rev. A. **45**, 8185 (1992)
10. M. Padgett, R. Bowman, Tweezers with a twist. Nat. Photon. **5**(6), 343–348 (2011)
11. D.G. Grier, A revolution in optical manipulation. Nature **424**(6950), 810–816 (2003)
12. J. Wang, J. Yang, I.M. Frazal, N. Ahmed, Y. Yan, H. Huang, Y. Ren, Y. Yue, S. Dolinar, M. Tur, E. Willner, Terabit free-space data transmission employing orbital angular momentum multiplexing. Nat. Photon. **6**(7), 488–496 (2012)
13. L. Qiu, H. Hu, Y. Zhao et al., Fiber optic temperature sensor using the orbital angular momentum and gaussian beams. Instrum. Sci. Technol. **45**(2), 123–136 (2017)
14. M. Turk, A. Pentland, Eigenfaces for Recognition. J. Cogn. Neurosci. **3**(1), 71–86 (1991)
15. S. Ramachandran, P. Kristensen, M.F. Yan, Opt. Lett. **34**, 2525 (2009)
16. Y. Yan, L. Zhang, J. Wang, J.-Y. Yang, I.M. Fazal, N. Ahmed, A.E. Willner, S.J. Dolinar, Opt. Lett. **37**, 3294 (2012)
17. Y. Li, L. Jin, H. Wu et al., Superposing multiple LP modes with microphase difference distributed along fiber to generate OAM mode. IEEE Photon. J. **9**(2), 1–9 (2017)
18. D. C. Ghiglia, M. D. Pritt, *Two-dimensional phase unwrapping theory, algorithms and applications* (Wiley, New York, 1998)